Merging tsunamis of the 2011 Tohoku-Oki earthquake detected over the open ocean

Y. Tony Song,[1] Ichiro Fukumori,[1] C. K. Shum,[2] and Yuchan Yi[2]

Received 23 December 2011; revised 6 February 2012; accepted 12 February 2012; published 8 March 2012.

[1] Tsunamis often travel long distances without losing power and severely devastate some coastal areas while leaving others with little damage. This unpredictable situation has been a major challenge for accurate and timely tsunami forecasting to facilitate early-warning and possible evacuations of affected coastal communities without disturbing the lives of others. Here we show evidence from satellite altimetry observations of the 2011 Tohoku-Oki earthquake-induced tsunami that sheds light on this issue. Three satellites observed the same tsunami front, and for the first time, one of them recorded a tsunami height about twice as high as that of the other two. Model simulations, based on the GPS-derived earthquake source and constrained by measurements of seafloor motions near the hypocenter, confirm that the amplified tsunami is one of several jets formed through topographic refraction when tsunamis travel along ocean ridges and seamount chains in the Pacific Ocean. This process caused the tsunami front to merge as it propagates, resulting in the doubling of the wave height and destructive potential in certain directions. We conclude that the potential of merging tsunamis should be emphasized in mapping tsunami hazards and assessing risk levels at key coastal facilities. **Citation:** Song, Y. T., I. Fukumori, C. K. Shum, and Y. Yi (2012), Merging tsunamis of the 2011 Tohoku-Oki earthquake detected over the open ocean, *Geophys. Res. Lett.*, *39*, L05606, doi:10.1029/2011GL050767.

1. Introduction

[2] Just 7 years after the devastating tsunami caused by the magnitude 9.2 Sumatra-Andaman earthquake on 26 December of 2004 and one year after that of the magnitude 8.8 Chilean Maule earthquake on 27 February of 2010, another destructive tsunami occurred resulting from a massive magnitude 9.0 earthquake that occurred at 14:46 Japan time (05:46 UTC) on 11 March of 2011, 160 km off Japanese Tohoku coast. The resulting destruction was a shock to all who watched the Japanese tragedy unfolded. A field survey reported an inundated tsunami height of about 40 meters in the Japanese coast after the event [*Mori et al.*, 2011]. Many people in the zones affected by the tsunami evacuated to safety, but others were not so fortunate. A total of 19,508 fatalities has been recorded [*Ando et al.*, 2011].

[1]Jet Propulsion Laboratory, California Institute of Technology, Pasadena, California, USA.
[2]Division of Geodetic Science, School of Earth Sciences, Ohio State University, Columbus, Ohio, USA.

0094-8276/12/2011GL050767

[3] Tsunamis not only devastate near-field coastal communities, but also travel long distances over ocean without losing much power to incur damage to far-field coastal regions. For example, the 1960 Chilean M9.5 earthquake, the largest earthquake ever recorded by instruments, generated a tsunami which incurred about 200 additional casualties in Japan and Hawaii, far away from the earthquake epicenter. On the other hand, fear of the far-reaching power of tsunamis has also caused many false alarms and unnecessary evacuations. For example, the 2010 Maule M8.8 earthquake triggered a basin-wide tsunami alert and caused evacuations in some Hawaiian and Japanese islands, but no destructive wave was found. All these incidents clearly indicate that there are still challenges in accurately forecasting either the near-field or the far-field tsunami hazards.

[4] An earthquake tsunami, usually originated from the fault line besides a continental slope, has two wave fronts: one directly run-ups to the continental slope and inundates the shore within about 30 minutes after the quake; while the other front propagates in the opposite direction over the deep ocean before inundating a far-field shore [*Satake*, 1995]. The waves that hit the Japanese coast from the 2011 Tohoku-Oki earthquake are the result of the near-field tsunami front, while the cross-ocean killer waves that hit Japan and Hawaii from the 1960 Chilean M9.5 earthquake are the consequence of the far-field tsunami front. For the near-field forecast, the challenge is to predict a tsunami's power and its extent early enough for issuing timely warnings to the local communities [*Song*, 2007; *Rabinovich et al.*, 2008; *Lomax and Michelini*, 2009; *Tsushima et al.*, 2009]. For the far-field forecast, the challenge is to determine those coastal communities that are in danger without disturbing the lives of others [*Yeh et al.*, 1994; *Titov et al.*, 2005a].

[5] During the last several decades, tsunami research, particularly tsunami modeling, has been focused on the far-field tsunami hazard because one could afford a considerable time lag when a tsunami propagates over the deep ocean before reaching shore [e.g., *Tang et al.*, 2008; *Wei et al.*, 2008]. Since the 1960 Chilean tsunami incident, scientists have theorized that ocean bottom topography could cause tsunami to merge in certain directions and the merging mechanism might be the culprit of those cross-ocean killer waves [*Woods and Okal*, 1987]. A more realistic numerical model of the 2004 Indian Ocean tsunami further demonstrated that tsunami waves could be amplified by trapping effect of mid-ocean ridges [*Titov et al.*, 2005b]. In general, wave and topography interactions have been extensively studied with numerical models [e.g., *Koshimura et al.*, 2008; *Kowalik et al.*, 2008]. However, observational evidence of the merging tsunamis has been elusive until now.

[6] Here we show evidence of merging tsunamis resulting from the 2011 Tohoku-Oki earthquake using satellite

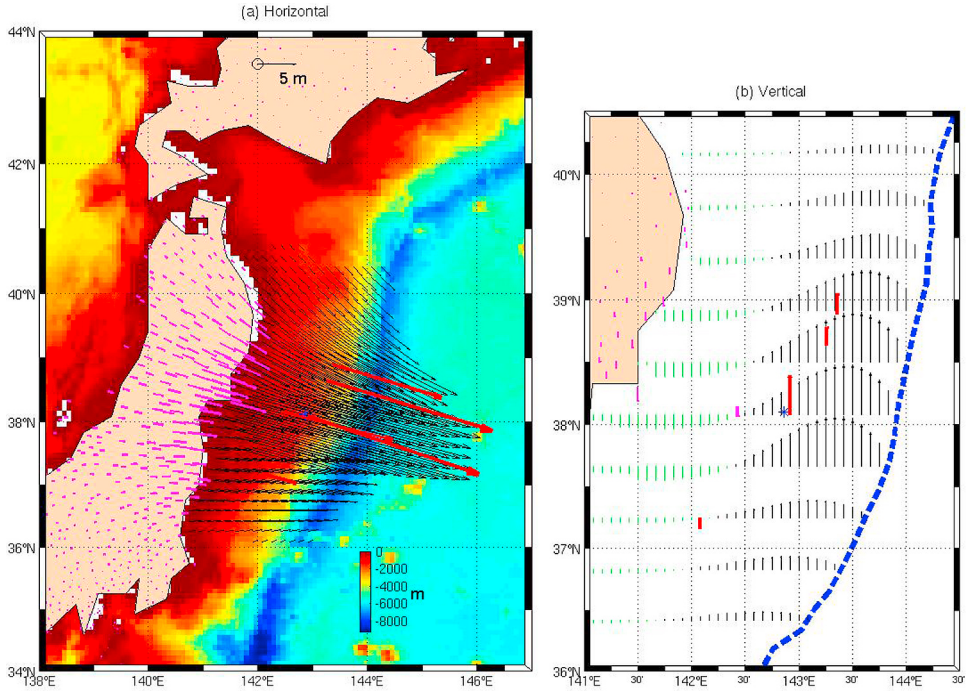

Figure 1. (a) Pink arrows are the GPS displacement of the ground motions (courtesy of ARIA team at the Jet Propulsion Laboratory and the California Institute of Technology). Black arrows (plotted every 5 points) are the horizontal displacement of the seafloor modeled from the land-based GPS data and compared with in-situ measurements (heavy red arrows) from *Sato et al.* [2011]. Color is ocean bathymetry in meters (color bar). (b) Same but for the vertical direction. The blue dashed-line is the trench. Note that the green arrows indicate subsidence and black arrows indicate uplift, which are also compared with *Sato et al.* [2011]. The arrow scale of 5 m applies to both directions. Star is the hypocenter.

altimetry observations. The NASA-Centre National d'Etudes Spaciales (CNES) Jason-1 satellite passed over the tsunami on March 11, as did two other altimetry satellites: the NASA-CNES Jason-2 and the European Space Agency's ENVISAT. All three satellites carry radar altimeters, which measure global sea level change with an accuracy of a few centimeters. Each satellite crossed the tsunami at different locations. Jason-2 and ENVISAT measured tsunami heights (from trough to peak) of 25 cm and 30 cm, respectively. But as Jason-1 passed over the ocean with undersea Mid-Pacific Mountains to the east, it captured a wave front measuring more than twice higher at 70 cm.

[7] To confirm the satellite-observed amplified waves are the long-hypothesized merging tsunamis, we have used model simulations based on independent data, including the Global Positioning System (GPS) data from the Geospatial Information Authority of Japan (GSI), and tsunami data from the NOAA's DART buoys. In the following section, we first derive the tsunami source from GPS data and compare it with undersea measurements from *Sato et al.* [2011]. Based on the GPS-derived tsunami source, we carry out a tsunami simulation and validate the model with data from DART buoys in section 3. We then show that satellite altimetry observations confirm the model prediction by matching the tsunami model along those satellite tracks in section 4. Discussions are given in section 5.

2. Tsunami Source

[8] Japan has an advanced near real-time network of GPS stations that is able to monitor the three dimensional ground motions across Japan. The GPS network, operated by the Geospatial Information Authority of Japan (GSI), consists of about 1200 stations with an average spacing of 20 kilometers over Japan that comprises the largest GPS monitoring array in the world [*Simons et al.*, 2011]. An animation of the GPS displacements as well as the related aftershocks is also available online (http://www.youtube.com/watch?v=1QCcVqZgNKw&NR=1). The GPS data enable the most complete, prompt and densest measurement of near-field ground motions ever for an earthquake with such a magnitude.

[9] Using the land-based GPS data and the empirical profile method of *Song* [2007], we have estimated the tsunami source, including the horizontal displacement and vertical uplift of the seafloor that are used as forcing mechanism for the resulting tsunami modeling [*Song et al.*, 2008; *Song and Han*, 2011]. Figure 1a shows the GPS measured velocities on the land (pink arrows) and the derived seafloor displacements (black arrows); while Figure 1b gives the corresponding vertical deformations, including subsidence of the land and uplift of the seafloor. The GPS-predicted seafloor motions have then been used to calculate the tsunami source energy, E_T, which includes both the potential energy due to the seafloor uplift (and subsidence) and the kinetic energy due to the horizontal displacements of the continental slope. The source energy also depends on the local topography and the rising-time of faulting, which is formulated by an empirical profile function: $E_T = f(\Delta E, \Delta N, \Delta U, \Delta t, h_x, h_y)$, where ΔE, ΔN, and ΔU are the eastward, northward, and upward seafloor displacements derived from nearby GPS stations, Δt is the rise-time of faulting,

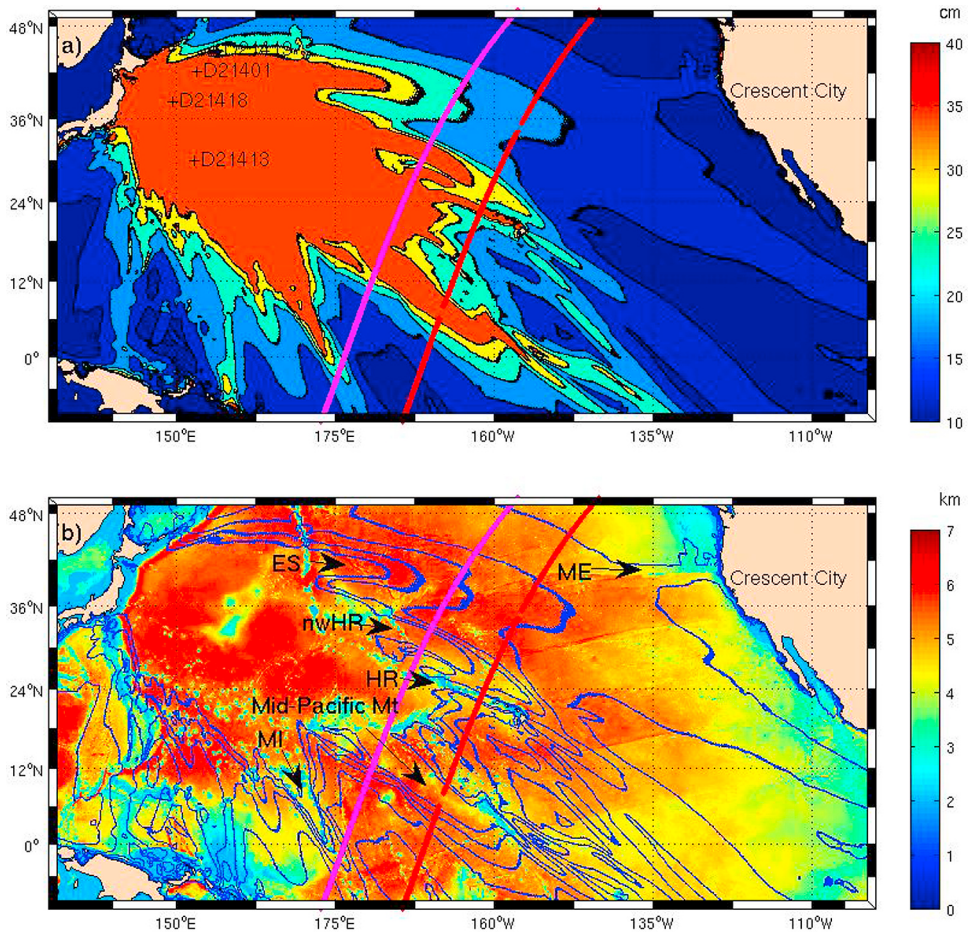

Figure 2. (a) Model tsunami maximum amplitude (color bar in cm) and the locations of DART buoys (crosses) and satellite ground tracks (red and pink lines), and (b) the contours of the tsunami maximum (blue lines) overlay on the ocean bathymetry (color bar in km). Black arrows indicate the tsunami jets formed from the corresponding topographic features: Emperor Seamounts (ES), northwest Hawaiian Ridge (nwHR), Hawaiian Ridge (HR), Mid-Pacific Mountains, Marshall Islands (MI), and Mendocino Escarpments (ME).

h_x and h_y are the eastward and northward slopes of the subfault surface, respectively [*Song et al.*, 2008]. Based on the linear wave theory in deep oceans (the square root of wave energy is proportional to the wave amplitude), the tsunami potentials (scales) can be determined from the GPS-derived seafloor motions and tsunami source energy [*Song*, 2007]

$$S_T = \log_{10} E_T - 10, \tag{1}$$

where S_T is the tsunami scale and the number 10 is chosen to range the scale from 1 to 10. We have estimated a tsunami source energy of 3.0×10^{15} Joule and a scale of 5.5 from the 2011 Tohoku-Oki earthquake. In comparing with the 2004 Sumatra-Andaman earthquake, the energy is about half of the 2004 Indian Ocean tsunami [*Song*, 2007]. The tsunami scale is a quantitative representation of tsunami height in deep oceans or its potential destructive force affecting coastal regions.

[10] The GPS-derived earthquake source has been compared with the undersea in-situ measurements of *Sato et al.* [2011], as shown in Figures 1a and 1b. It can be seen that there are some discrepancies. For example, the horizontal displacement from the model is about 20% less than the measurements. In the vertical, the model overestimates the two northern stations (KAMN and KAMS), but underestimates the other three stations (MYGW, MYGI and FUKU). It should be noted that the land-based GPS data and the model are mainly for the coseismic displacement (about 30 minutes); while Sato et al.'s measurements include both coseismic and post-seismic effects (surveyed from November 2010 to April 2011). The post-seismic slip does not contribute to the tsunami and is estimated to about only 10% of the coseismic slip [*Ozawa et al.*, 2011]. However, previous studies on other earthquakes reported that the post-seismic slip released a moment of up to ~30% of the main shock over several weeks [e.g., *Baba et al.*, 2006; *Chlieh et al.*, 2007]. Taking the post-seismic effect of this earthquake into account, our land-based GPS model agrees with the undersea measurements fairly well.

3. Tsunami Model and DART Buoy Data

[11] This GPS-derived tsunami source has been used to initialize a tsunami simulation, similar to our previous studies for the 2004 Sumatra-Andaman earthquake and the 2005 Nias Island earthquake [*Song*, 2007]. Figure 2a shows the model's maximum tsunami amplitude, illustrating

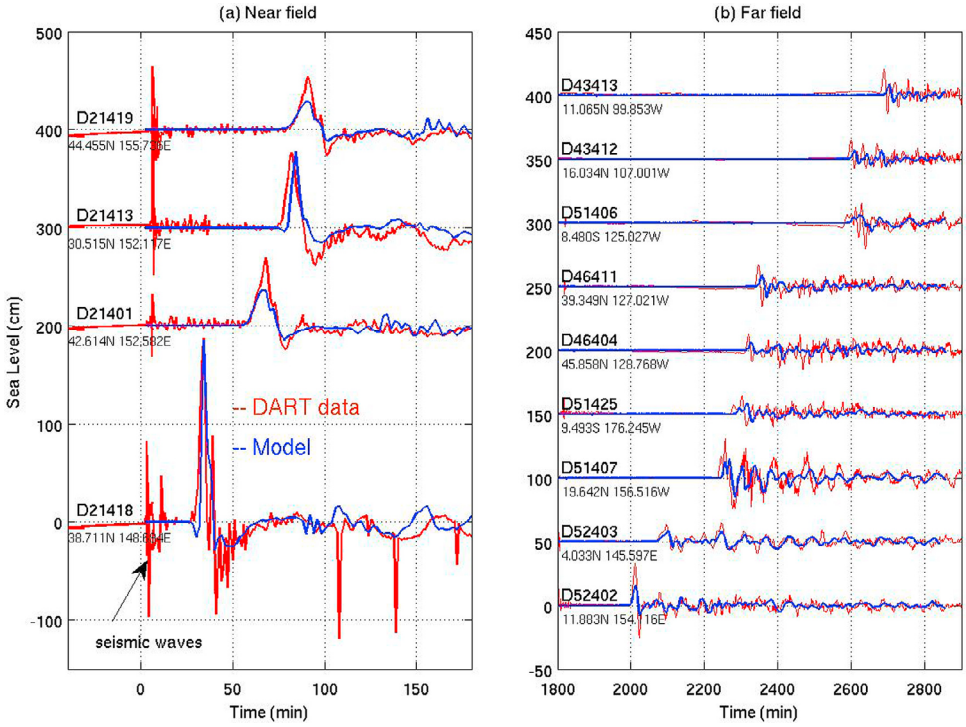

Figure 3. Comparison of the model tsunami (blue) with DART buoy measurements (red): (a) for those near-field buoys as marked in Figure 2a and (b) for those far-field buoys near Hawaii, California and Chile. The buoy numbers and their corresponding locations are given. The sharp spikes recorded by the buoys are seismic signals of the main earthquake and its aftershocks. Time in minutes starts from the initial time of the earthquake.

several narrow jets over the open ocean with larger amplitudes than elsewhere that converge the tsunami energy in some directions. Overlaying the contours of the maximum tsunami height over the ocean bathymetry shows each of the jets originating from a particular topographic feature (Figure 2b). These features are, for instance, the Emperor Seamounts (ES), the northwest Hawaiian Ridge (nwHR), the Hawaiian Ridge (HR), the Mid-Pacific Mountains, the Marshall Islands (MI), and the Mendocino Escarpment (ME). Note the jets continuing well beyond those topographic features. As the tsunami front passes a topographic ridge, a segment of the front would slow down due to the ridge's shallower depth and the wave front would curve towards the ridge on both sides due to refraction. The refraction causes the fronts to collide with each other and form a stable 'A' shape front as the tsunami passes along the ridge.

[12] To validate our GPS-based tsunami model, we have compared the simulated tsunami with data recorded by DART buoys (http://www.ndbc.noaa.gov/dar.shtml). Figure 3 compares the model with DART data at near-field and far-field stations, showing good agreement. At the buoy closest to the epicenter (DART21418), the tsunami height (from trough to peak) is about 2.5 meters (Figure 3a); while at other buoys further from the epicenter, the tsunami height is reduced to one meter and a few tens of centimeters in far-field (Figure 3b).

4. Satellite Altimetry Observations

[13] This tsunami propagation pattern in the deep ocean seems consistent with conventional view that the tsunami energy propagates from the source and radiates out approximately in a circle with diminishing amplitude. When the circle expands, the wave height decays because the same total energy is distributed over a larger area. Once the wave travels to shallower depth, its height is amplified with shorter wavelengths, sometimes inundating the coast when the resulting height is substantial [*Satake*, 1995]. In fact, the ocean bathymetry is complex; there are seamounts, ridges, and islands in the open ocean. These topographic features are responsible for the formation of these jets with amplified wave heights. Although numerical models have demonstrated some of the tsunami propagation features, obtaining observational evidence about tsunami's behavior in the open ocean has always been difficult. Particularly, observations of such amplification of tsunami fronts in the deep ocean have hitherto been lacking or elusive.

[14] On 11 March 2011, just after the main shock, three satellites, Jason-1, Jason-2, and ENVISAT carrying radar altimeters passed over the Pacific Ocean. As the tsunami fronts were rolling across the Pacific Ocean toward the American continent, these satellites recorded sea surface topography change associated with these tsunami waves, in addition to changes due to ocean circulation. Different from the DART buoys, the satellite observations in the open ocean represent continuous profiles of sea surface topography change. By comparing the satellite tracks with model simulations, we can determine those tracks that had observed the tsunami [*Song et al.*, 2005]. Of all the tracks over the Pacific Ocean during the tsunami period, three passes, Jason-1 pass 147, Jason-2 pass 21, and ENVISAT pass 419, match the tsunami's propagation in time and space. In particular, the two Jason satellites, separated from each other in space by about 1500 km, observed two dramatically

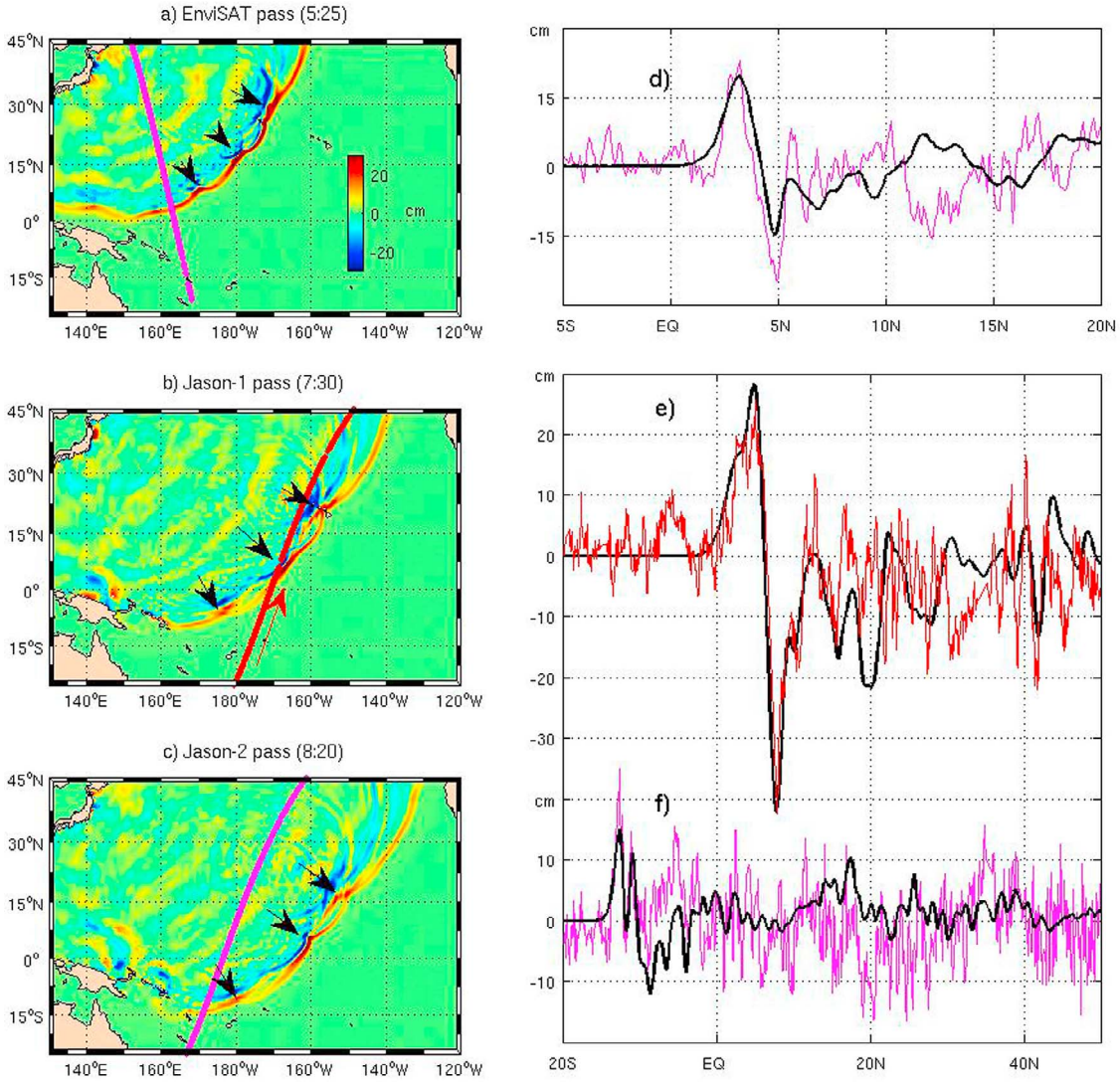

Figure 4. (a) ENVISAT pass at 5:25 hours after the quake, (b) Jason-1 pass at 7:30 hours after the quake, (c) Jason-2 pass at 8:20 hours after the quake, and (d–f) comparing model tsunami (black) with the satellite altimetry data along the passes, respectively. Black arrows indicate locations of merging tsunamis. Only the Jason-1 satellite, indicated by the red arrow, was at the right location and right time to catch the tsunami merge phenomenon.

different tsunami heights, which are the focus of the scientific discovery of this study, and are shown in Figures 4a–4f. It is noted that the tsunami height observed by Jason-1 (Figure 4e) is about twice as high as those observed by ENVISAT (Figure 4d) and by Jason-2 (Figure 4f) along the same tsunami front, suggesting the amplification of the tsunami height is a result of merging waves. Such spatially varying amplification would be difficult for a single in-situ instrument to record because of the limited width of the jets.

5. Discussions

[15] In summary, we have not only confirmed the existence of merging tsunamis that should be the focus for far-field tsunami forecast, but also demonstrated the feasibility of using real-time GPS data for near-field tsunami early warning [*Hammond et al.*, 2011; *Ohta et al.*, 2012]. The current tsunami warning system is based on early-estimated earthquake-moment magnitude primarily using seismic data to determine the potential of tsunami generations, but unfortunately, rapid estimate of earthquake's magnitude has not been successful. For example, the initial estimate of the March 11, 2011 earthquake was significantly smaller. Had the magnitude been correctly estimated initially, more lives could have been saved [*Ando et al.*, 2011]. Here, we have demonstrated an alternative approach using the existing Japanese GSI GPS network to infer seafloor displacement that determines the energy an undersea earthquake transfers to the ocean to generate a tsunami, instead of using of the earthquake's magnitude, which can more accurately and rapidly determine the tsunami power (scale). The basic steps are the following: First, locate an earthquake epicenter from seismometers (a few minutes after an initial quake); secondly, collect near-field GPS-derived land velocities and infer the seafloor motions (a few more minutes of latency are possible); and thirdly, calculate the tsunami-source energy or scale based on the GPS-predicted seafloor motions and local topography. If the oceanic energy scales greater

than a threshold, an initial warning can be issued. This approach had also been successfully tested in the 2010 Maule earthquake (http://www.jpl.nasa.gov/news/news.cfm?release=2010-198). It is noted that the land-based GPS data are collected in real-time by GSI which can be processed rapidly to compute near real-time ground motions with a latency of a few seconds and as accurate as few centimeters [*Bock et al.*, 2000]. Therefore, if for the prompt occurrence of the post-seismic slip, we can use these data to isolate the main shock (coseismic) to avoid complications by the post-seismic slip to compute the more exact tsunami source.

[16] In addition, the existence of the merging tsunamis suggests that far-field tsunami forecasting needs to consider not only local bathymetry, but also deep-ocean bottom topographic features that might have amplified tsunami run-ups. This extraordinary twice-amplification of tsunami height in the deep ocean, before the tsunami inundates the coastal region, would contribute to a tsunami's far-reaching and extended power with minimal energy dissipation. For example, Crescent City in California that lies along the extension of the Mendocino Escarpment has been one of the most frequently tsunami inundated cities along the California coast [*Kowalik et al.*, 2008]. In 1964, a tsunami generated from Alaska sent 20-foot waves crashing into Crescent City, killing 11 people. Both tsunamis of the 2006 magnitude 8.3 Kuril Islands earthquake and the 2011 Tohoku-Oki earthquake have caused serious damage to the coast of Crescent City, while only little damage was evident at other nearby regions. By better understanding how a tsunami interacts with topography, one may be able to more accurately predict merging tsunamis before they reach coastal communities. Similarly, in assessing risk levels for coastal nuclear power plants and oil refineries in earthquake and tsunami prone regions, one should consider not only their locations, but also the potential of merging tsunamis in the direction of an incoming tsunami.

[17] **Acknowledgments.** The research described here was conducted at the Jet Propulsion Laboratory, California Institute of Technology, under contracts with the National Aeronautics and Space Administration (NASA). The Ohio State University component of the research is supported under NASA's Physical Oceanography Program. We thank Alexander B. Rabinovich and four anonymous reviewers for their constructive comments, which have improved the paper. We thank the Geospatial Information Authority of Japan for providing the GPS data, NOAA for providing DART buoy data, and AVISO for the altimetry data.

[18] The Editor thanks the anonymous reviewers for their assistance in evaluating this paper.

References

Ando, M., M. Ishida, Y. Hayashi, and C. Mizuki (2011), Interviews with survivors of Tohoku earthquake provide insights into fatality rate, *Eos Trans. AGU*, *92*(46), 411–412, doi:10.1029/2011EO460005.

Baba, T., K. Hirata, T. Hori, and H. Sakaguchi (2006), Offshore geodetic data conducive to the estimation of the afterslip distribution following the 2003 Tokachi-oki earthquake, *Earth Planet. Sci. Lett.*, *241*, 281–292, doi:10.1016/j.epsl.2005.10.019.

Bock, Y., R. M. Nikolaidis, and P. J. de Jonge (2000), Instantaneous geodetic positioning at medium distances with the Global Positioning System, *J. Geophys. Res.*, *105*(B12), 28,223–28,253, doi:10.1029/2000JB900268.

Chlieh, M., et al. (2007), Coseismic slip and afterslip of the great Mw 9.15 Sumatra-Andaman earthquake of 2004, *Bull. Seismol. Soc. Am.*, *97*, S152–S173, doi:10.1785/0120050631.

Hammond, W. C., et al. (2011), Scientific value of real-time Global Positioning System data, *Eos Trans. AGU*, *92*(15), 125–126, doi:10.1029/2011EO150001.

Koshimura, S., Y. Hayashi, K. Munemoto, and F. Imamura (2008), Effect of the Emperor seamounts on trans-oceanic propagation of the 2006 Kuril Island earthquake tsunami, *Geophys. Res. Lett.*, *35*, L02611, doi:10.1029/2007GL032129.

Kowalik, Z., J. Horrilo, W. Knight, and T. Logan (2008), Kuril Islands tsunami of November 2006: 1. Impact at Crescent City by distant scattering, *J. Geophys. Res.*, *113*, C01020, doi:10.1029/2007JC004402.

Lomax, A., and A. Michelini (2009), Tsunami early warning using earthquake rupture duration, *Geophys. Res. Lett.*, *36*, L09306, doi:10.1029/2009GL037223.

Mori, N., T. Takahashi, T. Yasuda, and H. Yanagisawa (2011), Survey of 2011 Tohoku earthquake tsunami inundation and run-up, *Geophys. Res. Lett.*, *38*, L00G14, doi:10.1029/2011GL049210.

Ohta, Y., et al. (2012), Quasi real-time fault model estimation for near-field tsunami forecasting based on RTK-GPS analysis: Application to the 2011 Tohoku-Oki earthquake (Mw 9.0), *J. Geophys. Res.*, doi:10.1029/2011JB008750, in press.

Ozawa, S., T. Nishimura, H. Suito, T. Kobyashi, M. Tobita, and T. Imakiire (2011), Coseismic and postseismic slip of the 2011 magnitude-9 Tohoku-Oki earthquake, *Nature*, *475*, 373–376, doi:10.1038/nature10227.

Rabinovich, A. B., L. I. Lobkovsky, I. V. Fine, R. E. Thomson, T. N. Ivelskaya, and E. A. Kulikov (2008), Near-source observations and modeling of the Kuril Islands tsunamis of 15 November 2006 and 13 January 2007, *Adv. Geosci.*, *14*, 105–116, doi:10.5194/adgeo-14-105-2008.

Satake, K. (1995), Linear and nonlinear computations of the 1992 Nicaragua earthquake tsunami, *Pure Appl. Geophys.*, *144*, 455–470, doi:10.1007/BF00874378.

Sato, M., T. Ishikawa, N. Ujihara, S. Yoshida, M. Fujita, M. Mochizuki, and A. Asada (2011), Displacement above the hypocenter of the 2011 Tohoku-Oki earthquake, *Science*, *332*, 1395, doi:10.1126/science.1207401.

Simons, M., et al. (2011), The 2011 magnitude 9.0 Tohoku-Oki earthquake: Mosaicking the megathrust from seconds to centuries, *Science*, *332*, 1421–1425, doi:10.1126/science.1206731.

Song, Y. T. (2007), Detecting tsunami genesis and scales directly from coastal GPS stations, *Geophys. Res. Lett.*, *34*, L19602, doi:10.1029/2007GL031681.

Song, Y. T., and S. C. Han (2011), Satellite observations defying the long-held tsunami genesis theory, in *Remote Sensing of the Changing Oceans*, edited by D. L. Tang, pp. 327–342, Springer, Berlin, doi:10.1007/978-3-642-16541-2_17.

Song, Y. T., C. Ji, L.-L. Fu, V. Zlotnicki, C. K. Shum, Y. Yi, and V. Hjorleifsdottir (2005), The 26 December 2004 tsunami source estimated from satellite radar altimetry and seismic waves, *Geophys. Res. Lett.*, *32*, L20601, doi:10.1029/2005GL023683.

Song, Y. T., L.-L. Fu, V. Zlotnicki, C. Ji, V. Hjorleifsdottir, C. K. Shum, and Y. Yi (2008), The role of horizontal impulses of the faulting continental slope in generating the 26 December 2004 tsunami, *Ocean Modell.*, *20*, 362–379, doi:10.1016/j.ocemod.2007.10.007.

Tang, L., V. V. Titov, Y. Wei, H. O. Mofjeld, M. Spillane, D. Arcas, E. N. Bernard, C. Chamberlin, E. Gica, and J. Newman (2008), Tsunami forecast analysis for the May 2006 Tonga tsunami, *J. Geophys. Res.*, *113*, C12015, doi:10.1029/2008JC004922.

Titov, V. V., F. I. Gonzalez, E. N. Bernard, M. C. Eble, H. O. Mojfeld, J. C. Newman, and A. J. Venturato (2005a), Real-time tsunami forecasting: Challenges and solutions, *Nat. Hazards*, *35*, 35–41, doi:10.1007/s11069-004-2403-3.

Titov, V. V., A. B. Rabinovich, H. O. Mofjeld, R. E. Thomson, and F. I. González (2005b), The global reach of the 26 December 2004 Sumatra Tsunami, *Science*, *309*, 2045–2048, doi:10.1126/science.1114576.

Tsushima, H., R. Hino, H. Fujimoto, Y. Tanioka, and F. Imamura (2009), Near-field tsunami forecasting from cabled ocean bottom pressure data, *J. Geophys. Res.*, *114*, B06309, doi:10.1029/2008JB005988.

Wei, Y., E. Bernard, L. Tang, R. Weiss, V. Titov, C. Moore, M. Spillane, M. Hopkins, and U. Kanoolu (2008), Real-time experimental forecast of the Peruvian tsunami of August 2007 for U.S. coastlines, *Geophys. Res. Lett.*, *35*, L04609, doi:10.1029/2007GL032250.

Woods, M. T., and E. A. Okal (1987), Effect of variable bathymetry on the amplitude of teleseismic tsunamis: A ray-tracing experiment, *Geophys. Res. Lett.*, *14*(7), 765–768, doi:10.1029/GL014i007p00765.

Yeh, H., P. Liu, M. Briggs, and C. Synolakis (1994), Propagation and amplification of tsunamis at coastal boundaries, *Nature*, *372*, 353–355, doi:10.1038/372353a0.

I. Fukumori and Y. T. Song, Jet Propulsion Laboratory, California Institute of Technology, 4800 Oak Grove Dr., Pasadena, CA 91109, USA. (tony.song@jpl.nasa.gov)

C. K. Shum and Y. Yi, Division of Geodetic Science, School of Earth Sciences, Ohio State University, 125 S. Oval Mall, Columbus, OH 43210, USA.